The time structure of atmospheric Cerenkov light in extensive air showers

1977 J. Phys. A: Math. Gen. 10 441

(http://iopscience.iop.org/0305-4470/10/3/016)

J. Phys. A: Math. Gen., Vol. 10, No. 3, 1977. Printed in Great Britain.

The time structure of atmospheric Čerenkov light in extensive air showers

E Böhm†, G Bosia‡, G Navarra‡ and O Saavedra‡

† Institut für Reine und Angewandte Kernphysik, Universitat Kiel, West Germany
‡ Laboratorio di Cosmo-Geofisica del CNR, Corso Fiume 4, 10133 Torino, Italy

Received 25 May 1976, in final form 18 October 1976

Abstract. The time structure of atmospheric Čerenkov light has been measured by narrow-angle detectors in extensive air showers with a time resolution of 0·15 ns. From comparison with particle density observations in the same showers it is deduced that the temporal shape is a measure of the lateral structure of the particle shower disc rather than of the longitudinal shower development.

1. Introduction

In recent years much effort has been devoted to improving our knowledge of the longitudinal development of extensive air showers (EAS), a subject of decisive importance in the interpretation of EAS in terms of physical parameters. Different methods and various shower components have been explored in this respect. Measurements on atmospheric Čerenkov light have been proposed as rather promising ways to obtain such information. Several groups have performed calculations (Sitte 1970, Castagnoli *et al* 1967b, Rieke 1969, Bosia *et al* 1972c) which directly correlate the arrival time distribution of the Čerenkov light in detectors of small opening angle to the shower development. Measurements on the temporal distribution of Čerenkov light were first reported by Boley *et al* (1961) and Castagnoli *et al* (1967a). In these experiments Čerenkov light detectors only were used and results on the average thickness of the shower disc were obtained. Later on an experimental proof concerning the relation between the Čerenkov light arrival time and the longitudinal shower development was undertaken by Bosia *et al* (1970), but still with poor data on the behaviour of the particle shower. Furthermore, a complex time structure in the Čerenkov light pulse has sometimes been observed in this experiment, the explanation of which was not clear. The present experiment was designed to give more detailed experimental results on the behaviour of atmospheric Čerenkov light in EAS and to explain substructures in the arrival time distribution (Bosia *et al* 1976).

There exist different mechanisms which cause time delays in observation of atmospheric Čerenkov light:

(*a*) the velocity differences between particles and light due to the refractive index of air and its variation through the atmosphere;
(*b*) the path length differences between light produced at different points in the shower;
(*c*) the finite disc thickness and the curvature of the disc.

The velocity delays (*a*) are able to give direct information on the longitudinal development, but the delay of light with respect to particles is small for atmospheric depths at mountain altitudes. This small delay is masked by the structure of the disc (*c*) (the disc thickness is known to be a few nanoseconds at least, Woidneck and Bohm 1975). Path length differences (*b*) become important if the opening angle of the detector is large or the shower direction does not coincide with the direction of view of the detector. In this case light is mainly observed from particles scattered into that direction (Jelley 1967). Since the scattering angle of particles is larger than the Čerenkov light emission angle for the majority of shower particles, it is likely that the main contribution is due to the delay from path length differences. Therefore the arrival time distribution of Čerenkov light is linked to the particle distribution in the shower plane from the position seen by the detector at different times.

The aim of the present paper is to show which of the delay mechanisms is the most important in producing the arrival time profiles of atmospheric Čerenkov light as observed in showers of size 10^4–10^6 particles, close to the core.

2. Apparatus and method

At the Pic du Midi (Pyrenees, 2860 m) an air shower array consisting of thirteen scintillation counters of 0·25 m^2 each (van Staa *et al* 1973) has been operated together with seven detectors for atmospheric Čerenkov light observation (figure 1). Each Čerenkov light detector consisted of a parabolic mirror of 90 cm diameter, aluminized and housed in a blackened and thermalized wooden box. The reflectivity of the mirror has been measured to be better than 90% for $\lambda > 2500$ Å. In the focus of the mirror (f/65 cm) a photomultiplier was mounted. The seven detectors were aligned optically to the zenith within 0·2°. Three of the detectors were equipped with fast photomultipliers XP 1210 to measure the arrival time distribution of Čerenkov light; the other four were equipped with photomultipliers 56 AVP, and were used to determine the arrival

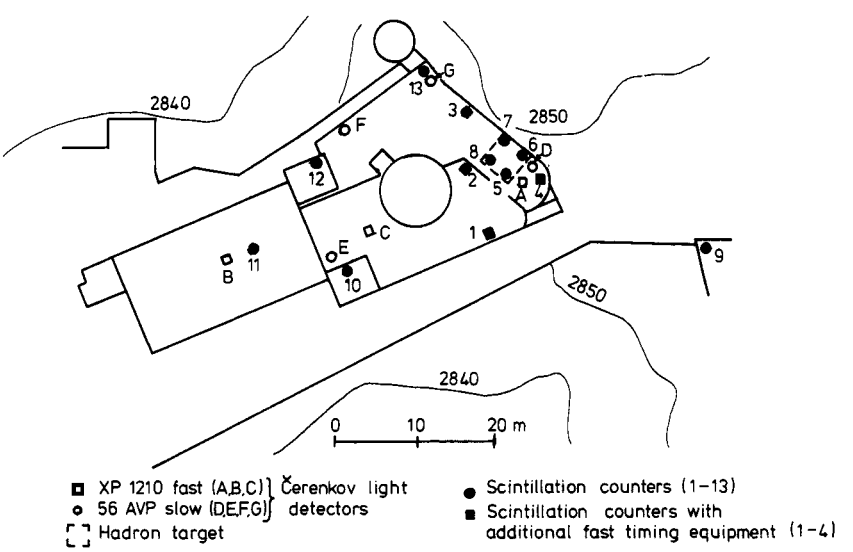

Figure 1. Detector configuration.

direction of the shower from the arrival time of the light. Filters (mainly Schott UG 11) have been used to reduce the noise of the night sky. The full opening angle of detectors was 3°. Figure 2 shows the angular resolution of one of the detectors: the current in the photomultiplier caused by the night sky background light shows the passage of stars in the direction of view of the detector (Marangoni *et al* 1973).

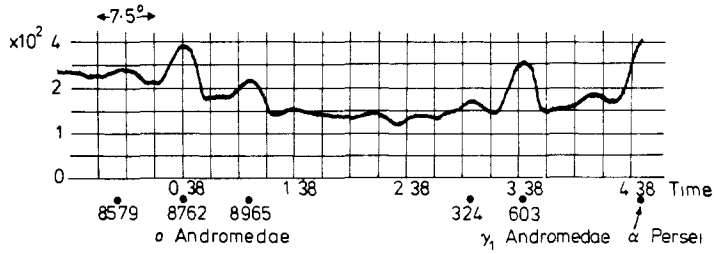

Figure 2. Dark-current measurement of night sky with XP 1210 (10 September 1972).

The pulses of the fast multipliers were directly (DC coupling) displayed on a Tektronix 519 (2 GHz) with 30 ns total beam length; the pulses of the slow detectors were displayed on a Tektronix 547 after pulse shaping and mixing with suitable delays. Single TV frames of all four oscillograms were recorded by a television camera (Isocon EEV/P880) and stored on magnetic tape (Ampex VR74403) (Marangoni *et al* 1973). The photographs were digitized off-line (Bosia *et al* 1972b) with a stepwidth of 0·15 ns and 0·05 V on the fast beams (the beam thickness being 0·15 V, standard deviation). The step width in time on the slow beam was 1·1 ns.

The gain of the fast multipliers has been checked with a Čerenkov light radiator (plexyglass) by using cosmic ray particles (Bosia *et al* 1972a) and has been found to agree with the specifications. The dependence of the gain on the power supply has been measured with light-emitting diodes (Monsanto MV4). During the measurement the voltage on the HV power supply was set individually for each fast multiplier, depending on the dark current, and the gain was checked by calibrated diodes (MV4) mounted in front of each multiplier. The time resolution has been determined by the Čerenkov radiator and cosmic ray particles. A typical time response to a δ-like time function of the input pulse is given in figure 3.

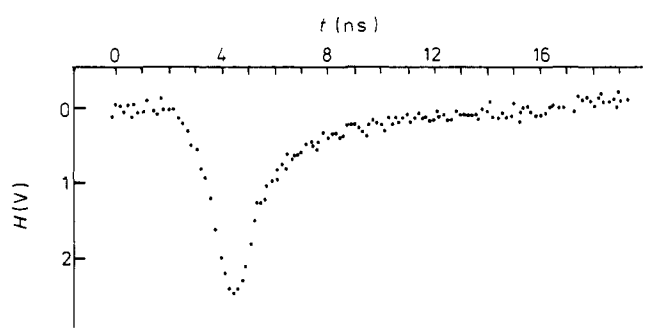

Figure 3. Time response of XP 1210 for a δ distribution at input. Pulse height 2·5 V, rise-time 1·4 ns, full width at half maximum 1·8 ns.

Showers have been recorded with two substantially different triggering requirements:

(i) threefold coincidence in the fast Čerenkov light detectors (pulse height larger 0·5 V, equivalent to about 100 photons in a δ pulse response) and:

(a) a fourfold coincidence in the slow Čerenkov light detectors, or

(b) at least one particle, or

(c) a cascade in the hadron detector (more than 30 particles in a 0·1 m^2 scintillation counter, equivalent 30 GeV threshold)

—high efficiency in Čerenkov light detection;

(ii) fivefold coincidence in the particle detectors (two or more particles in detectors 1–4, more than 15 particles in one of the detectors 5–8) together with at least one Čerenkov light signal—high efficiency in detecting particle showers.

Particle data were stored on punched paper tape (dead-time 10 s), Čerenkov data on video tape (dead-time 1·5 s).

The analysis is based on measurements during eleven nights with 13 800 events in 116 hours. In 56 events full information on the particle shower as well as for the Čerenkov light shower was obtained. These events are of particular interest for a comparison of the two shower components analysed in this paper. Figure 4 shows an example of the data set for one event. From the particle data record, information on the shower parameters was obtained by a least-squares fit. Shower size N, core position x_0, y_0 and, in sufficiently large showers, the arrival direction (θ, ϕ) were determined. The accuracy in the parameters depends on the shower size and the core location: it is greatest at the position of highest particle detector density (scintillation counters 1–8). For large showers ($N \geq 10^5$) the error in core position is about 1 m in the centre and

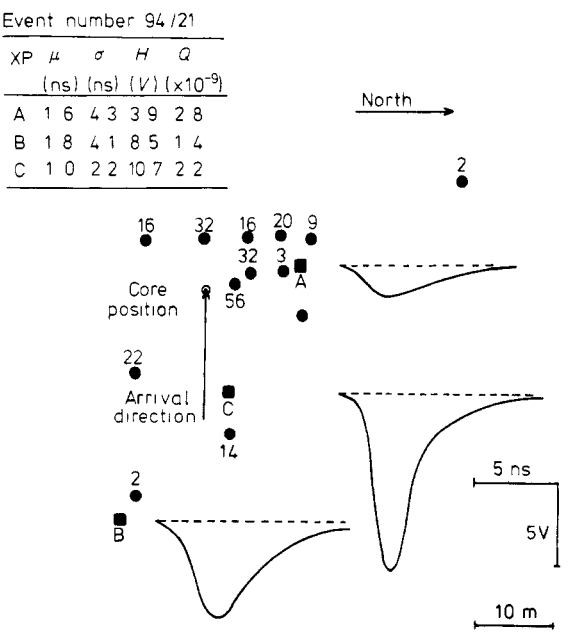

Figure 4. Example of data set of recorded showers; Q is the number of electrons collected at the anode of the photomultipliers (uncorrected for different photomultiplier gains $g_A : g_B : g_C = 1 : 0{\cdot}7 : 0{\cdot}5$).

exceeds 10 m at the edges of the detector array. For small showers ($N \lesssim 10^4$) it becomes difficult to assign shower parameters to individual events, and average values from statistical samples may be obtained. From the recorded Čerenkov light pulses a few characteristic parameters have been extracted to describe the pulse shape $n_{ph}(t)$: the pulse height at maximum H, the rise-time μ (from 10% to 90% of the pulse height H), the full width at half maximum σ and the integral of the time distribution of the pulse $Q = \int n_{ph}(t)\, dt$.

3. Phenomenological results

The various triggering requirements provide different kinds of showers. Particle requirements preferentially select showers not yet absorbed and the core being not far from the detectors, showers with sufficiently large primary energy or an extremely low starting point are recorded. The Čerenkov light trigger provides primary particle events of smaller energy, the shower of which may already have been absorbed or the core may have fallen far from the particle detectors. From a phenomenological point of view these different shower characteristics should exhibit themselves in the measured quantities. Thus, before comparing the experimental results of particle and Čerenkov light measurements in individual events some phenomenological description of the experimental data is presented for the two components separately.

The rise-time and halfwidth of the detected Čerenkov light pulses from Čerenkov light triggers are shown in figure 5 and compared with the time resolution obtained from the measurements as described in § 2. The average values of pulse width and rise-time in showers are clearly larger than the resolution. The halfwidth is often larger than the total delay as is to be expected from the longitudinal shower development (4·9 ns in total at 2890 m altitude, due to the refractive index of the atmosphere).

In figure 6 the integral spectrum of the photon content observed by the individual detectors is presented. At large photon densities, where there is no bias due to the triggering requirements (threefold in Čerenkov light) the spectra have a slope of about -3, while $-1{\cdot}5$ would be expected (Gierdes *et al* 1975) if the photon density Q were proportional to the primary energy E_0, and the lateral distribution function were independent of energy E_0, $Q(r) = E_0 f(r)$. But this dependence only holds if the particle shower does not reach the observation level, otherwise a dependence $Q \sim E_0^{\alpha}$ with $\alpha < 1$ would appear, which causes qualitatively a steepening of the photon density spectrum compared with the slope of the primary energy spectrum, as observed here. This can be taken as an indication that the Čerenkov light is coming mainly from showers which have not yet been fully absorbed at the observation level.

Figure 7 shows the shower size distributions as recorded with the different triggering conditions. The slopes at large sizes are rather close to each other. In all showers above about 10^6 particles Čerenkov pulses are observed irrespective of the arrival direction, even in the detectors with small opening angles (see also appendix 3). Taking the decrease in the rate of events to be due to the difference of solid angle in 'particle shower' and 'Čerenkov light' observation, the ratio of rates should be $R_{rate} = 1 - \cos^{n+1}\theta_0$ if a zenith angle distribution $I(\theta)\, d\omega = I_0 \cos^n \theta\, d\omega$ is assumed. For $R_{rate} = 50$, from figure 7, and $n = 6$ the opening angle for Čerenkov light observation turns out to be $\theta_0 = 4°$, larger than the actual opening angle $\theta_0 = 1{\cdot}5°$ (see § 2) and the Čerenkov light emission angle $\theta_c = 1{\cdot}3°$. Thus, showers with their arrival directions within the cone of observation of the Čerenkov light detectors are not the only

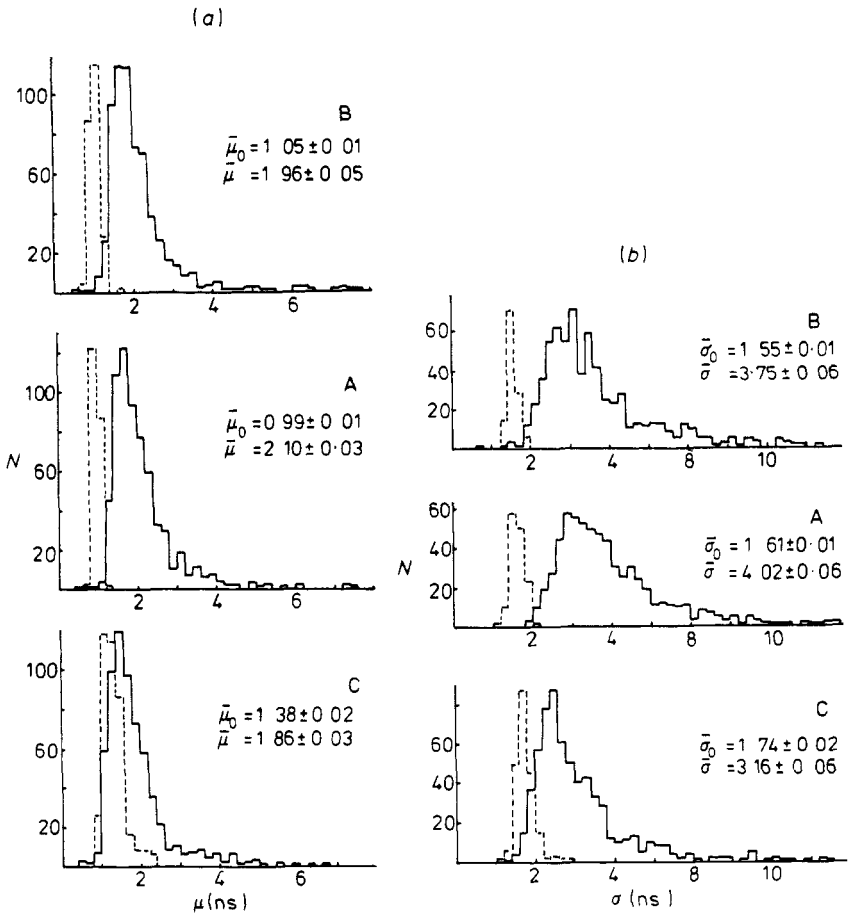

Figure 5. Distributions of (*a*) rise-time and (*b*) halfwidth Čerenkov light pulses (full lines) observed in showers compared with the resolution of the detectors (broken lines).

contributors to the shower rate. The arrival direction of the Čerenkov light seems to be determined by the scattering angle of the particles rather than by the Čerenkov light emission angle.

The results discussed so far allow a qualitative description of the behaviour of Čerenkov light and the particles in the air shower. Since a large number of showers arrive inclined with respect to the cone of observation of the Čerenkov light detector, the main contribution to the detected Čerenkov light comes from particles scattered out of the shower direction into the direction of view of the Čerenkov light detectors. In addition the particles are not yet absorbed before they reach the observation level, thus the Čerenkov light is produced rather close to the detectors and not high in the atmosphere. This is confirmed by a comparison of the pulse width in showers with no detected particle and in showers with eleven or more particle detectors triggered (figure 8). The average width is larger in showers with many particles, and the distribution in halfwidth is broader, due to the larger inclination of shower arrivals causing longer delays due to path length differences. This picture is also supported by a measurement of the change of rate of Čerenkov light with the zenith angle of direction of the detectors

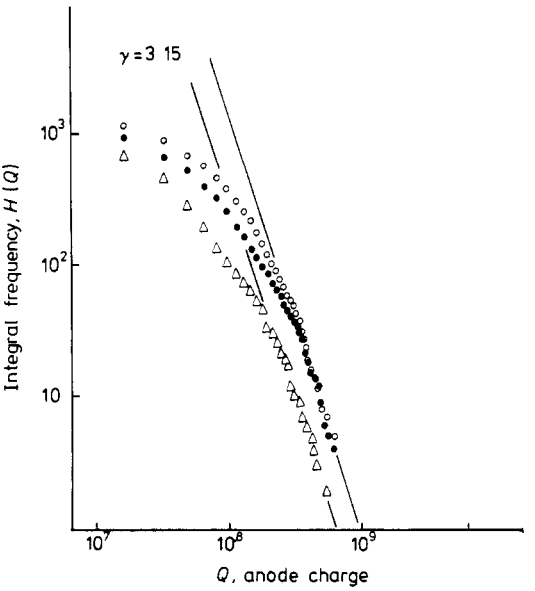

Figure 6. Čerenkov light photon density distribution (not corrected for detection bias). Data recorded 15–17 October 1971 from photomultipliers: ○, A; ●, B; △, C.

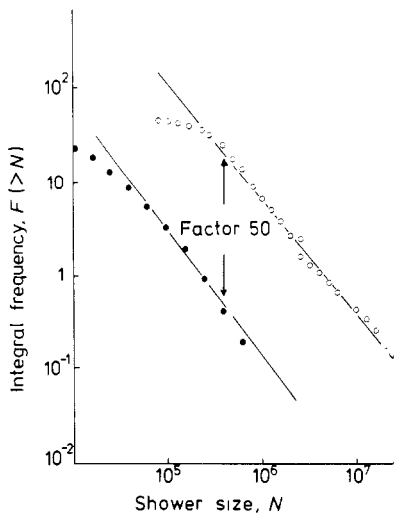

Figure 7. Shower size distributions for differing triggering requirements (not corrected for detection efficiency). ○, particle showers recorded 18–20 October 1971; ●, Čerenkov light showers recorded 15–17 October 1971.

(see appendix 4). With this basic concept the data have been subjected to a more detailed analysis. The main emphasis has been put on the interpretation of events with sufficient information about both components measured, particles and atmospheric Čerenkov light.

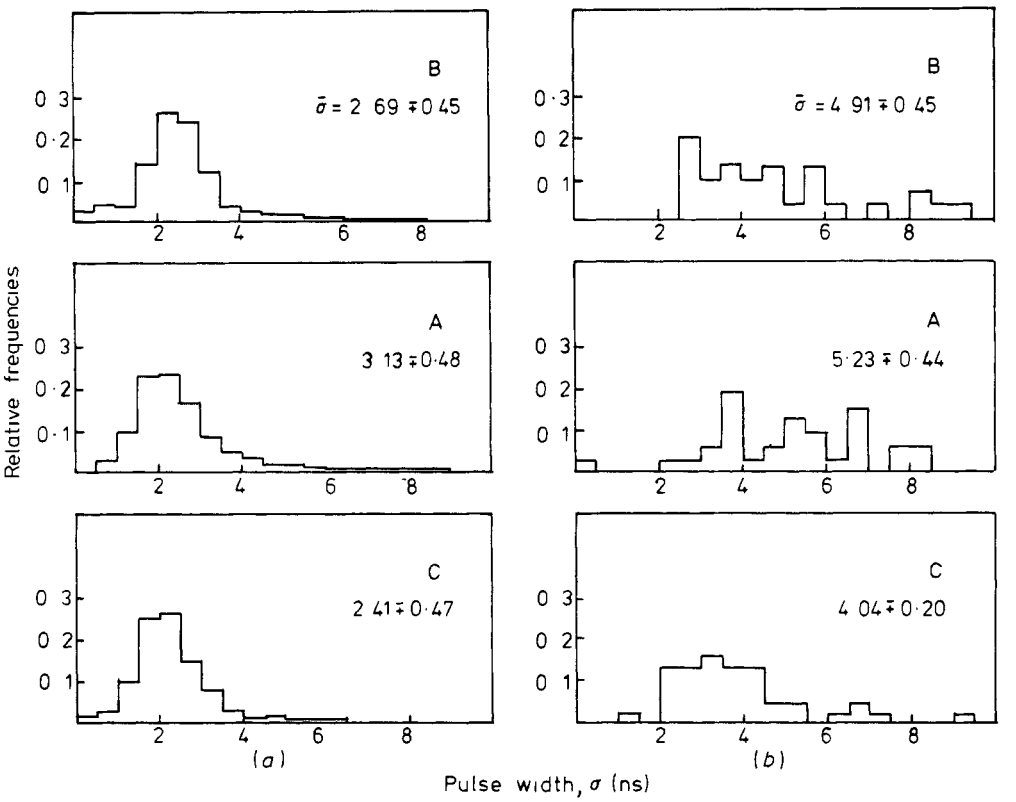

Figure 8. Čerenkov pulse width in Čerenkov light triggers depending on the number of scintillators triggered k: (*a*) $k = 0$; (*b*) $k \geq 11$.

4. Model and applications

For this purpose a model has been developed (Böhm *et al* 1975), which relates the photon density of atmospheric Čerenkov light to the longitudinal and lateral density distributions of electrons (see appendix 1). This model is an extension of a model used earlier by Malos *et al* (1962). The arrival time of the Čerenkov light is a measure of the position of production of the light, the number of photons is a measure of the electron density at that position. The relation is unique in the limit of a flat disc, infinitely thin. For known behaviour of the particle shower, the arrival time distribution of the Čerenkov light can be calculated by applying the model. But the shower parameters can also be obtained from the Čerenkov light time profile by a maximum likelihood fit, if the showers are assumed to possess average characteristics, relating to the scattering of particles, disc structure and curvature, longitudinal development and lateral structure. The data used for this further analysis are given in appendix 1.

For the following analysis showers have been selected from the Čerenkov light trigger (arrival time distributions in three detectors) with at least six of the total thirteen particle detectors triggered. In these events the shower parameters as derived from the particle measurements are sufficiently accurate to be used as a reference for the time profile analysis.

Figure 9 shows examples of the best fits of the observed Čerenkov light pulse shape to the model, simultaneously in all three detectors A, B and C (see figure 1), and a comparison with the particle data. The agreement between measured and calculated pulse shape is fairly good, but the model cannot describe every detail in the pulse shape (figure 9(*b*)). The lateral distribution as calculated from the best-fit parameters differs from the particle densities recorded in absolute scale but is in good agreement regarding the slope. Figure 10 compares the shower sizes determined from the particle measurements and from the best fit in Čerenkov light profile. A correlation is to be seen but there is large scatter. Assuming average shower behaviour (i.e. average distributions in many dimensions, see figure 12) causes large fluctuations in the parameters obtained

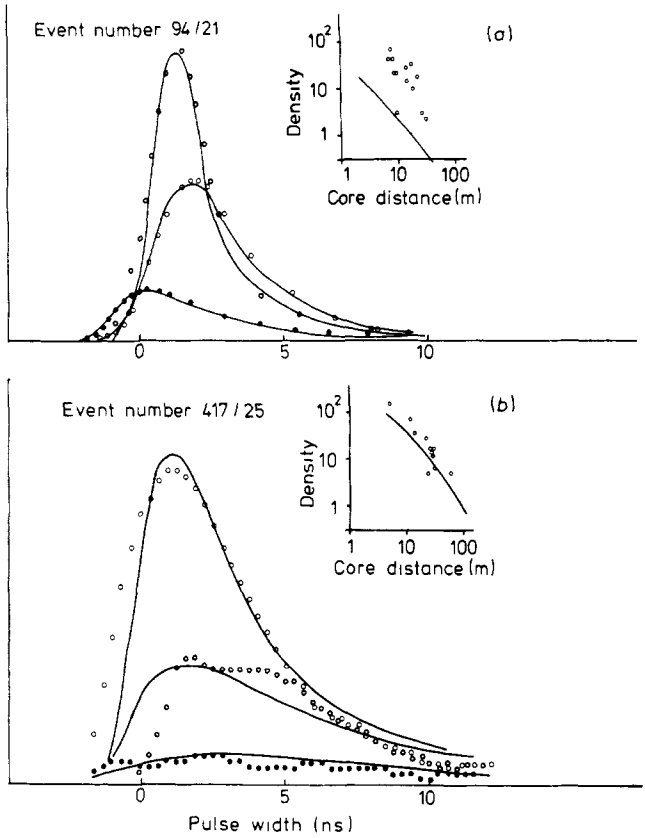

Figure 9. Examples of least-squares fits of observed Čerenkov light arrival time distributions. Full curves are calculated fits, while the experimental points ●, ⊙, ○ are from detectors A, B and C respectively. The data sets for parts (*a*) and (*b*) are:

Part	Type of data	θ	ϕ	X	Y	lg N
(*a*)	Particle	9	268	− 8	−5	5·3
	Čerenkov	5·4	268	− 8·5	− 3·3	4·5
(*b*)	Particle	15	2	−18	−28	5·8
	Čerenkov	11	326	−18	−28	5·8

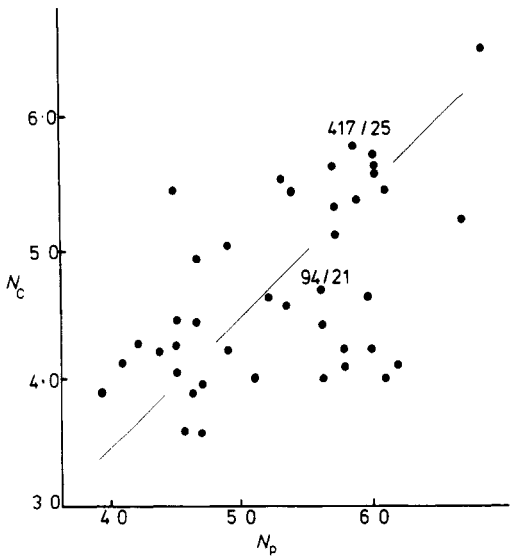

Figure 10. Correlation between shower size determined from particle data (N_p) and Čerenkov light detectors (N_C), correlation coefficient $r = 0{\cdot}33 \pm 0{\cdot}14$, 417/25 and 94/21 events from figure 9.

from a least-squares fit, when compared with the properties of individual showers. In addition, the special geometry in the positions of the Čerenkov light detectors A, B and C (they are nearly on one line) limits the accuracy in the determination of shower parameters.

In figure 11 the zenith angles, determined from the data of the slow Čerenkov light detectors only (D–G, see figure 1) making use of the model ($\Delta t = (d/c)\tan(\theta/2)$), are related to the arrival directions from particle data. The scatter in the diagram is comparable to the errors in the single values ($\Delta\theta_C \simeq \Delta\theta_p \simeq 3°$); the result is incompatible with propagation of the shower within the core of the Čerenkov light detectors ($\theta_C \simeq \theta_p \simeq 0°$).

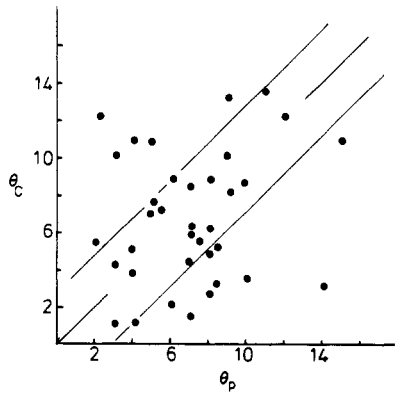

Figure 11. Comparison of EAS arrival zenith angles determined from particle data (θ_p) and slow Čerenkov light detectors (θ_C), correlation coefficient $r = 0{\cdot}20 \pm 0{\cdot}16$.

The distribution of the azimuth angle of arrival direction is in agreement with the model assumed. There are a large number of events with the core passing all detectors and thus reaching the maximum pulse height in all of them (see figure 12).

5. Burst trigger

For a few hours triggering by high energy particles ($E_b \geq 30$ GeV, see van Staa *et al* 1974) was used. The aim was to find out whether Čerenkov light might be useful in surviving-particle experiments. Such experiments, to detect primary particles which have passed through the atmosphere to the observation level without interaction provide a good way of measuring the mean free path (Aguirre *et al* 1975) and the charge of high energy cosmic rays. In 16 hours 9 events were observed with no particle, but accompanied by Čerenkov light. A qualitative discussion of these events is given in appendix 2. The Čerenkov light seems to be more efficient than particles for detecting absorbed showers in surviving-particle experiments. In high energy hadron experiments in cosmic rays (trigger) Čerenkov light (and/or particles) may provide a possible means of separating, at least on the average, residual primaries from secondary particles.

6. Trigger by a particle shower

If a particle shower is detected the core is close to the centre of the array preferentially and the particle density is large compared with that in Čerenkov light triggers. In nearly all events only one Čerenkov light detector responds. In these events it cannot be excluded that shower particles strike the photomultiplier directly simulating a Čerenkov light pulse from the atmosphere (see appendix 3).

7. Conclusions

To obtain information on the longitudinal development of EAS from the arrival time of atmospheric Čerenkov light by using Čerenkov light detectors of small opening angle is problematic, even when care is taken to avoid contributions caused by path length differences from different points of production. Due to the scattering of shower particles there is a sufficient number of particles moving in the direction of view of the detector, even in showers not propagating in this direction, to produce detectable Čerenkov light. In this case arrival time differences are caused, despite the precautions mentioned, by path length differences (between light and particles from various positions in the shower). To analyse the arrival time distribution in terms of the longitudinal development, the arrival direction of the shower has to be known independently with accuracy better than 0·2° (see figure 13) coinciding with the direction of view of the detector. Thus the information provided by the arrival time of Čerenkov light in EAS is not on the longitudinal development, but on the particle density of the shower, at points corresponding to the time of arrival of the light. The arrival time measurements offer the possibility of making a continuous scan of the lateral particle distribution, which has an advantage over the sampling method, necessary with particle detectors, usually applied in EAS research.

Acknowledgments

The authors gratefully acknowledge the use of facilities at the Observatoire du Pic du Midi; especially they would like to thank Dr A Cachon, who has been very helpful during the installation and operating time of the experiment. The continuous interest of Professor C Castagnoli is also gratefully acknowledged.

Part of this work has been supported by the Deutsche Forschungsgemeinschaft, under grants Tr11/6 and Bo469/1.

Appendix 1

A.1 Calculation of arrival time of Čerenkov light

The number of Čerenkov light photons emitted on the line element ds at P passing through a detector of area F at D (figure 12) is given by:

$$dN_{ph} \sim \frac{F}{h^2+r'^2} N(P) f(\theta, \theta') \cos\theta r' \, dr' \, d\phi \left(1-\frac{1}{n^2}\right) ds \tag{A.1}$$

(see, e.g., Bosia *et al* 1972c) where $N(P)$ is the number of shower particles at P; $f(\theta, \theta')$ is their angular distribution and n is the refractive index of the atmosphere at P (it is assumed that the Čerenkov light from each particle is radiated in its forward direction). The Čerenkov light produced at P is delayed with respect to the shower disc arriving at P by t, assuming a refractive index $n = 1+\eta_0 \exp(-h/h_0)$ (see, e.g., Jelley 1967), with:

$$ct = [(h^2+r'^2)^{1/2} - h\cos\theta + r'\sin\theta\cos\phi] + \{\eta_0 h_0[1-\exp(-h/h_0)] \times (h^2+r'^2)^{1/2}/h\} + [(R_e^2-r_D^2)^{1/2} - (R_e^2-r_P^2)^{1/2}]. \tag{A.2}$$

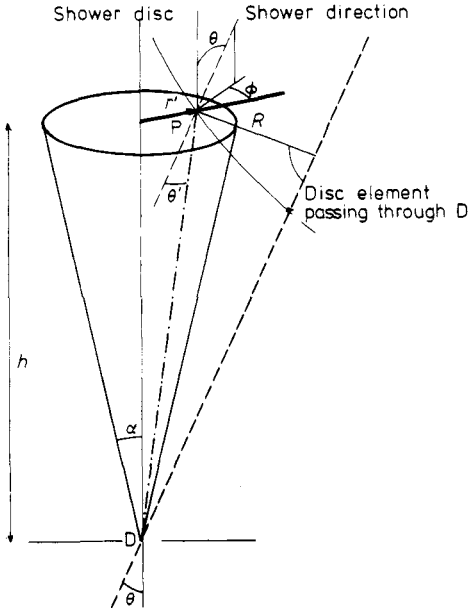

Figure 12. Geometry used for calculating the arrival time distribution of Čerenkov light.

The first term gives the delay due to path length differences, the second term the contribution from the atmospheric refractive index, the third term arises because of the curvature of the shower disc (R_e), it gives the delay between particles in the disc passing through P and D. r_P and r_D are the core distances of P and D respectively. The number of photons arriving in D at time t can be calculated by integrating (A.1) for t = constant. In a shower with an extended disc the delay given by (A.2) is the average delay t of the Čerenkov light emitted at P, the time delay distribution $g(t)$ of particles in the disc has to be superimposed on the arrival time of the average disc, leading to:

$$N_{ph}(t) \sim \int_{t-\tau>0} N(P)g(t-\tau)f(\theta, \theta')\frac{F}{h^2+r'^2}\cos\theta r'\,dr'\,d\phi\left(1-\frac{1}{n^2}\right)ds \qquad (A.3)$$

with $c\tau = c\bar{t} - [R_e - (R_e^2 - r_D^2)^{1/2}] - \Delta_0$, where Δ_0 is the advance of the shower front with respect to the mean disc in the core. At time τ the shower front passes P.

A.2 Approximations

For $r' \ll h$ (A.1) reduces to:

$$ct = h(1-\cos\theta) + \eta_0 h_0[1-\exp(-h/h_0)] + (R_e^2 - r_D^2)^{1/2} - (R_e^2 - r_P^2)^{1/2}.$$

An example of the time delay in the dependence on zenith angle is shown in figure 13 for fixed height and for fixed impact R (see figure 12). There is a minimum in delay at about 1°, at smaller angles delays due to velocity differences are dominant, while at larger zenith angles the path length differences become more important. Equation (A.3)

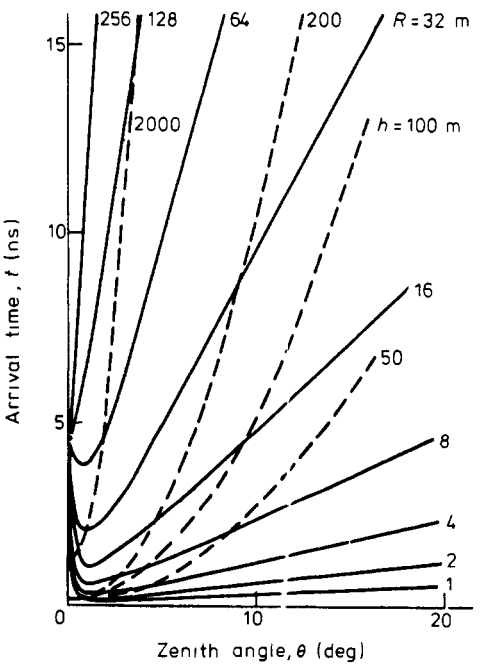

Figure 13. Dependence of the arrival time on zenith angle θ for $R_e \to \infty$; parameters: production height H, impact $R = H/\sin\theta$ (m).

reduces to:

$$N_{\mathrm{ph}}(t) \sim F\alpha^2 \cos\theta f(\theta) \int_{t-\tau>0} N(h) g(t-\tau)(1-1/n^2)\, \mathrm{d}h.$$

Conceptually the arrival time distribution can be described in the following way ($\theta > 1°$, see figure 14): the Čerenkov light detector looks along a line through the shower, the arrival direction of which is inclined with respect to this line. Along the projection of this line into the shower plane, the lateral distribution of particles is scanned. The pulse height at time t is proportional to the particle density at the position corresponding to time t. In this simple picture the pulse height is:

$$N_{\mathrm{ph}}(t) \sim N(r)c/(1-\cos\theta); \qquad (x-x_0)\tan(\theta/2) = ct; \qquad r^2 = x^2 + y_0^2$$

from which a rough estimation of the shower parameters is possible. The part of the lateral distribution scanned depends on the arrival direction of the shower and the position of the core with respect to the detector. Applying equation (A.2) the experimentally obtained time structure of atmospheric Čerenkov light in showers of known particle behaviour has been analysed. $h \ll h_0$ can be assumed and $N(h)$ has been taken to be exactly the lateral distribution (Nishimura–Kamata, in the Greisen approximation). Furthermore it has been taken that:

$R_e = 600$ m	Woidneck *et al* (1971)
$\sigma_r = 0{\cdot}5(1+r/60)^{2{\cdot}5}$ ns	Thielert and Wiedecke (1964)
$\Delta_0 = 3{\cdot}2$ ns	Woidneck *et al*(1975)
$g(t) \sim t^a \exp(-bt)$	
$b = (\bar{t}-\tau)/\sigma_r^2$; $a = b(\bar{t}-\tau)-1$; σ_r disc thickness	
$h_0 = 7900$ m; $\eta_o = 2{\cdot}9\times10^{-4}$	Jelley (1967)
$f(\theta,\theta')\,\mathrm{d}\omega \approx \exp[-(\theta-\theta')/\theta_0]\,\mathrm{d}\omega$, $\theta_0 = 3^0$	Sitte (1970)
($\theta = 3°$ at a core distance $r = 0{\cdot}5$ in Molière units)	

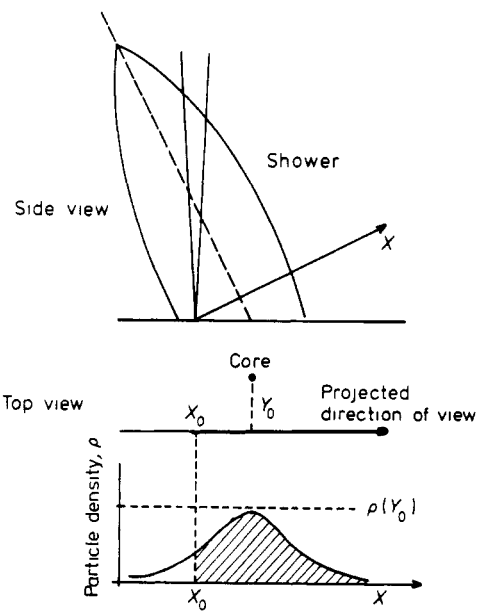

Figure 14. Concept of pulse shape interpretation.

Appendix 2. Burst trigger

To trigger the apparatus by high energy particles not necessarily accompanied by a particle shower or Čerenkov light a scintillator counter was mounted 3 m underneath the hadron target (see van Staa *et al* 1974). If more than 30 particles passed the 30×30 cm^2 counter all the other detectors were read out by the digitizing system and the data were stored.

356 high energy particles (bursts) were observed in 16 hours (22·2 per hour), 75 of which were coincident with at least one electron; 11 were accompanied by Čerenkov light, two of which were also accompanied by particles.

To check the compatibility with the known behaviour of high energy cosmic rays the experimental results were compared with simple model calculations. The flux of residual primary nucleons of energy E at depth x_0 is, assuming a superposition model for heavy primaries of mass A with energy being shared equally between the nucleons:

$$n_A(E)\,\mathrm{d}E = AS \sum_n P_n(x_0)(EA/\eta^n)^{-\gamma} A\,\mathrm{d}E/\eta^n.$$

$P_n(x_0)$ is the probability for a nucleon to suffer n interactions before reaching the observation level having energy $E = \eta^n E_0/A$ where η is the elasticity per interaction; $H(E_0)\,\mathrm{d}E_0 = SE_0^{-\gamma}\,\mathrm{d}E_0$ has been assumed for the primary spectrum. Using a Poissonian distribution P_n the flux becomes:

$$n_A(E)\,\mathrm{d}E = S\{A\,\exp[-x_0(1-\eta^{\gamma-1})/\lambda_\mathrm{p}] - \exp(-x_0/\lambda_\mathrm{p})\} A^{-\gamma+1} E^{-\gamma}\,\mathrm{d}E$$

if at least one particle interacts once. The average primary energy to produce a particle of energy E is:

$$E_A = EA \frac{A\,\exp(x_0\eta^{\gamma-2}/\lambda_\mathrm{p}) - 1}{A\,\exp(x_0\eta^{\gamma-1}/\lambda_\mathrm{p}) - 1}.$$

The threshold primary energy is:

$E_A^\mathrm{t} = AE$ for heavy particles

$E_\mathrm{p}^\mathrm{t} = E/\eta$ for protons.

The contribution from secondaries of the first generation, the only one considered important, is:

$$n'_A(E)\,\mathrm{d}E = \int_0^{x_0} n_A(E_1, x) n_\mathrm{s}(E_1) \exp[-(x_0 - x)/\lambda_\mathrm{s}](\mathrm{d}E_1/\mathrm{d}E)\,\mathrm{d}E\,\mathrm{d}x/\lambda_\mathrm{p} \qquad \text{(A.4)}$$

for a multiplicity law $n_\mathrm{s} = mE_1^\alpha$ and the produced particles sharing E_1 equally: $E_1 = [3mE/2(1-\eta)]^{1/(1-\alpha)}$. The average primary energy to produce a secondary of energy E in the first interaction is:

$$\bar{E}_A = AE^{1/(1-\alpha)} F(\lambda_\mathrm{p}, \lambda_\mathrm{s}, A, \eta, \gamma)$$

where F is a function coming from the integration of equation (A.4) with respect to x.

The threshold energy is:

$$E'_A = AE_1.$$

The calculations have been performed taking:

$$H(E_0)\,dE_0 = 2{\cdot}25E_0^{-2{\cdot}65}\,dE_0\ \text{cm}^{-2}\text{s}^{-1}\text{sr}^{-1}\text{GeV}^{-1} \qquad \text{(Kempa } et\ al \text{ 1973)}$$

$$m = 2;\ \alpha = 1/4;\ \eta = 0{\cdot}5;\ \lambda_p = 80\ \text{g cm}^{-2};\ \lambda_s = 120\ \text{g cm}^{-2}.$$

The calculated frequencies of bursts as a function of the energy are plotted in figure 15 for protons and iron primaries together with the measured flux, and for different

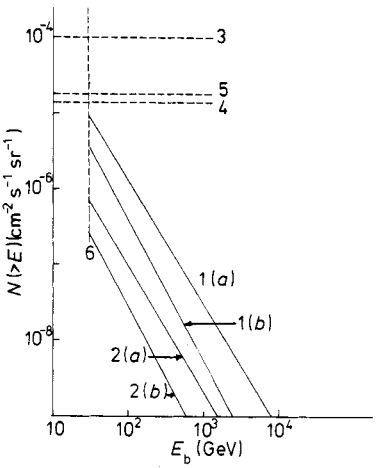

Figure 15. Calculated energy spectrum of bursts compared with measured frequencies (θ quoted is assumed for opening angle of the detector). The numbers labelling the various lines refer to: 1, protons; 2, iron primaries (where (*a*) refers to residual primaries and (*b*) to secondaries) ⊙ measured flux 3, detectors B and C, $\theta = 1{\cdot}5°$; 4, detectors B and C, $\theta = 4°$; 5 detector B only, $\theta = 20°$. 6, threshold burst energy.

assumptions concerning the opening angle of the detectors. In figure 16 the threshold energy and the mean primary energy are plotted; also included are the experimental points. The primary energy has been determined from the Čerenkov light pulses by applying the calculations of Zatsepin and Chudakov (1962). The burst energy has been obtained from the burst size assuming a conversion factor of 1 GeV/particle (this is a lower limit to the energy because of the angular spread of the produced particles and the geometrical configuration in detection). From the energy considerations of figure 16 we might conclude that the observed particles are secondary particles from a primary proton beam or residual nucleons from heavier primaries. This interpretation does not fit in with figure 15. If, however, one keeps in mind that the burst energy may be underestimated even residual primary protons may be marginally assumed as the detected particles.

With better energy determination in the burst energy and in the primary energy it should be possible to distinguish between residual primaries and secondary particles, at least on the average, in an experiment like the one discussed here.

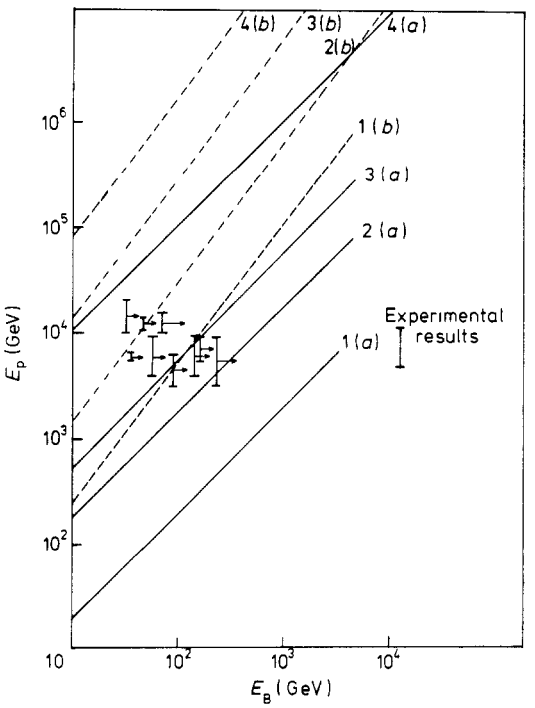

Figure 16. Calculated relation between burst energy and primary energy, and experimental results. The numbers labelling the various lines refer to protons: 1, E'; 2, $\bar{E}$ and iron primaries: 3, E'; 4, $\bar{E}$ where (*a*) refers to residual primaries and (*b*) to secondaries.

Appendix 3. Shower triggers and Čerenkov light

Assuming a Poissonian density distribution, the probability that no particle is observed on the area F where the average density of particles is ρ, is $\exp(-\rho F)$ and to find at least one particle is $1-\exp(-\rho F)$. If n events have been recorded with average densities $\rho_i (i = 1, \ldots, n)$, $k = \Sigma_{i=1}^{n} [1-\exp(-\rho_i F)]$ particles should be observed. Taking the area of the photomultiplier $F = 13{\cdot}8$ cm^2 and the particle density, as observed in the particle detector closest to the Čerenkov light detector in events triggered by the particle array without any additional requirement, the expected number of events with a 'Čerenkov signal' is in detector A:69, B:41, C:31; to be compared with 49, 23, 23 respectively detected in 590 triggers.

Special measurements have been performed to ascertain the pulse shape if the 'Čerenkov light' signal is produced by a particle traversing the photomultiplier. A scintillation counter close to the cathode assures the passage of a particle through a multiplier with darkened cathode. The pulse shape is rather regular and close to the shape for δ pulses (see figure 4). Figure 17 shows the distribution in pulse width obtained in this run; the pulse width in events with a trigger from a particle shower (included in figure 17) is on the average nearly as short, but has a longer tail. This shows that an appreciable number of the Čerenkov light pulses observed should have been produced directly by particles in the multiplier. Thus, observing atmospheric Čerenkov light in EAS close to the shower core, where the particle density is high, care has been taken in the interpretation of Čerenkov light signals.

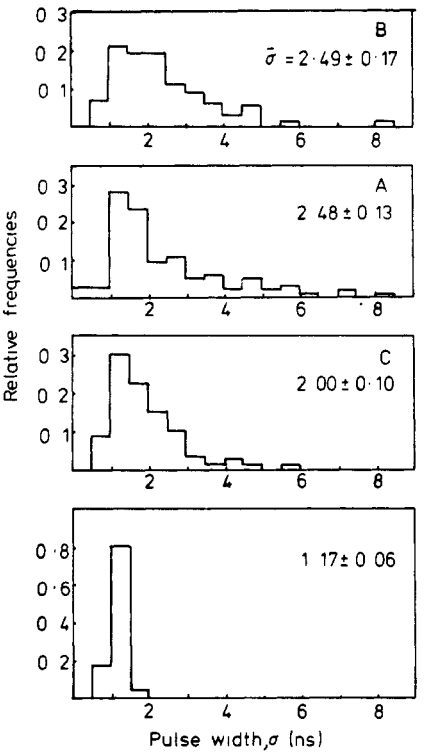

Figure 17. Distribution of halfwidth of Čerenkov light pulses observed in showers triggered by particles compared with 'pulses' from particles passing the phototube (bottom diagram).

Appendix 4. Zenith angle dependence of Čerenkov light

A special run has been performed for 14 hours to measure the zenith angle dependence of the atmospheric Čerenkov light. Two fast Čerenkov light detectors as described in § 2, with the same directions of view at zenith angle θ, and close to each other, have been run in coincidence.

Figure 18 shows the dependence in rate of events on the zenith angle, which is very close to that obtained for particle showers in this experiment, supporting the model as given in appendix 1. A different zenith angle dependence is expected if the shower is propagating in the cone of the detectors:

$$f(\theta) \approx \cos\theta \exp(-x_0/x \cos\theta) \tag{A.5}$$

where the first factor describes the change of amount of detected light with distance from production, the second the light absorption ($x_0 = 730$ g cm^{-2} observation level, $x = 790$ g cm^{-2} absorption length of light, Allen 1964).

Figure 19 shows the halfwidth of the observed Čerenkov light pulses in dependence on zenith angle. If the model (appendix 1) holds, the number of events with an angle α with respect to the direction of view of the detector is:

$$n(\alpha) \approx \exp(-\alpha/\alpha_0)\, d\omega \cos^n(\theta + \alpha).$$

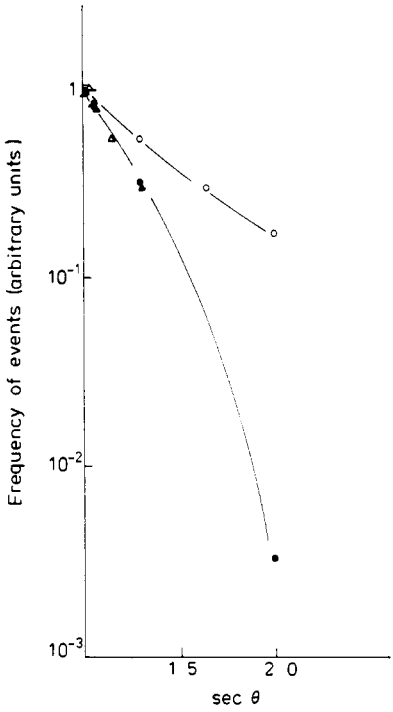

Figure 18. Zenith angle dependence of frequency of events for different experimental conditions. ●, Čerenkov light showers; △, particle showers; ○, expected from equation (A.5).

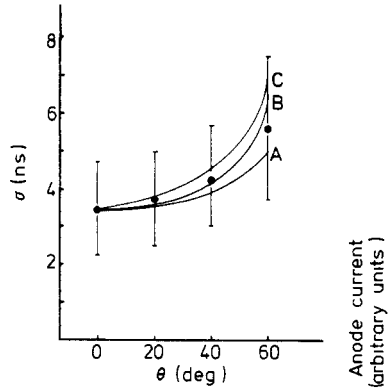

Figure 19. Average halfwidth in dependence on inclination of the Čerenkov light detectors. Curve A, $n = 4$; B, $n = 5$; C, $1/\cos\theta$.

The halfwidth for events observed with angle α is:

$$\sigma \propto \tan(\alpha(\theta)/2) \qquad \text{(see appendix 1)}$$

The mode of $n(\alpha)$ has been used to calculate the halfwidth, as included in figure 19. If the delay of the light is due to the refractive index $\sigma \approx \eta_0 h_0/c \cos\theta$ would be expected. From the halfwidth no decision on the model to be used can be obtained, but the result is in agreement with the expectations from the model given in appendix 1.

References

Aguirre C, Trepp A, Mejia G R, Murakami K, Kamata K, Toyoda Y, Maeda T, Yokoyama C, MacKewon P K, Suga K, Uchino K and Kaneko T 1975 *Nuovo Cim.* B **27** 263

Allen C W 1964 *Astrophysical Quantities* (London: Athlone Press)

Böhm E, Holtrupp G, Bosia G, Navarra G, Saavedra O and Cachon A 1975 *Proc. 14th Int. Conf. on Cosmic Rays, Munich* vol. 8 (München: Max Planck Institut für Extraterrestriche Physik) p 3046

Boley F I, Baum J H , Palsedge J A and Pereue J H 1961 *Phys. Rev.* **124** 1205

Bosia G, Castagnoli C, Marangoni G, Navarra G, Raspollini G and Saavedra O 1972a *Nuovo Cim.* B **9** 177

Bosia G, Marangoni G, Maringelli M and Navarra G 1972b *Nucl. Instrum. Meth.* **105** 117

Bosia G, Maringelli M and Navarra G 1972c *Nuovo Cim.* B **9** 201

Bosia G, Navarra G, Saavedra O and Böhm E 1976 in the press

Castagnoli C, Dardo M and Penengo P, 1967b *Phys. Rev.* **160** 1186

Castagnoli C, Locci M A, Picchi P and Verri G 1967a *Nucl. Phys.* B **2** 369

Gierdes C, Hartman D, Fau C Y and Weeks T C 1975 *Proc. 14th Int. Conf. on Cosmic Rays, Munich* vol. 8 (München: Max Planck Institut für Extraterrestriche Physik) p 3040

Jelley J V 1967 *Progress in Elementary Particles and Cosmic Rays* vol. 9 (Amsterdam: North Holland) p 41

Kempa J, Wdowczyk J and Zujewska E 1973 *Proc. 13th Int. Conf. on Cosmic Rays, Denver* (Denver: University of Denver) p 2145

Malos J, Millar D D and Wallace C S 1962 *J. Phys. Soc. Japan* **17** *Suppl.* A3 114

Marangoni G, Maringelli M, Raspollini G and Saavedra O 1973 *Proc. 13th Int. Conf. on Cosmic Rays, Denver* (Denver: University of Denver) p 2754

Rieke G H 1969 *Smithsonian Astrophysical Observatory Special Report* 301

Sitte K 1970 *Acta Phys. Sci. Hung.* **29** *Suppl.* 3 389

van Staa R, Aschenbach B and Böhm E 1974 *J. Phys. A: Math., Nucl. Gen.* **7** 135

Thielert R and Wiedeke L 1964 *Z. Phys.* **179** 199

Woidneck C P and Böhm E 1975 *J. Phys. A: Math. Gen.* **8** 997

Woidneck C P, Böhm E, Trumper J and De Villiers E J 1971 *Proc. 12th Int. Conf. on Cosmic Rays, Hobart* vol. 3 (Hobart: University of Tasmania) p 1038

Zatsepin G T and Chudakov A E 1962 *Sov. Phys.-JETP* **15** 1126